Supplemental Materials

Toxoplasma gondii serine hydrolases regulate parasite lipid mobilization during growth and replication within the host

Ouma Onguka[1], Brett M. Babin[1], Markus Lakemeyer[1], Ian T. Foe[1], Neri Amara[1], Stephanie M. Terrell[1,4], Kenneth M. Lum[2], Piotr Cieplak[3], Micah J. Niphakis[2], Jonathan Z. Long[1,4], and Matthew Bogyo[1,5]

[1]Department of Pathology, Stanford University School of Medicine, Stanford, CA 94305, USA

[2]Lundbeck La Jolla Research Center, San Diego, CA 92121, USA

[3] Infectious & Inflammatory Disease Center, Sanford Burnham Prebys Medical Discovery Institute, La Jolla, CA 92037, USA

[4]Stanford ChEM-H, Stanford University, Stanford, CA 94305, USA

[5]Department of Microbiology and Immunology, Stanford University, Stanford, CA 94305, USA

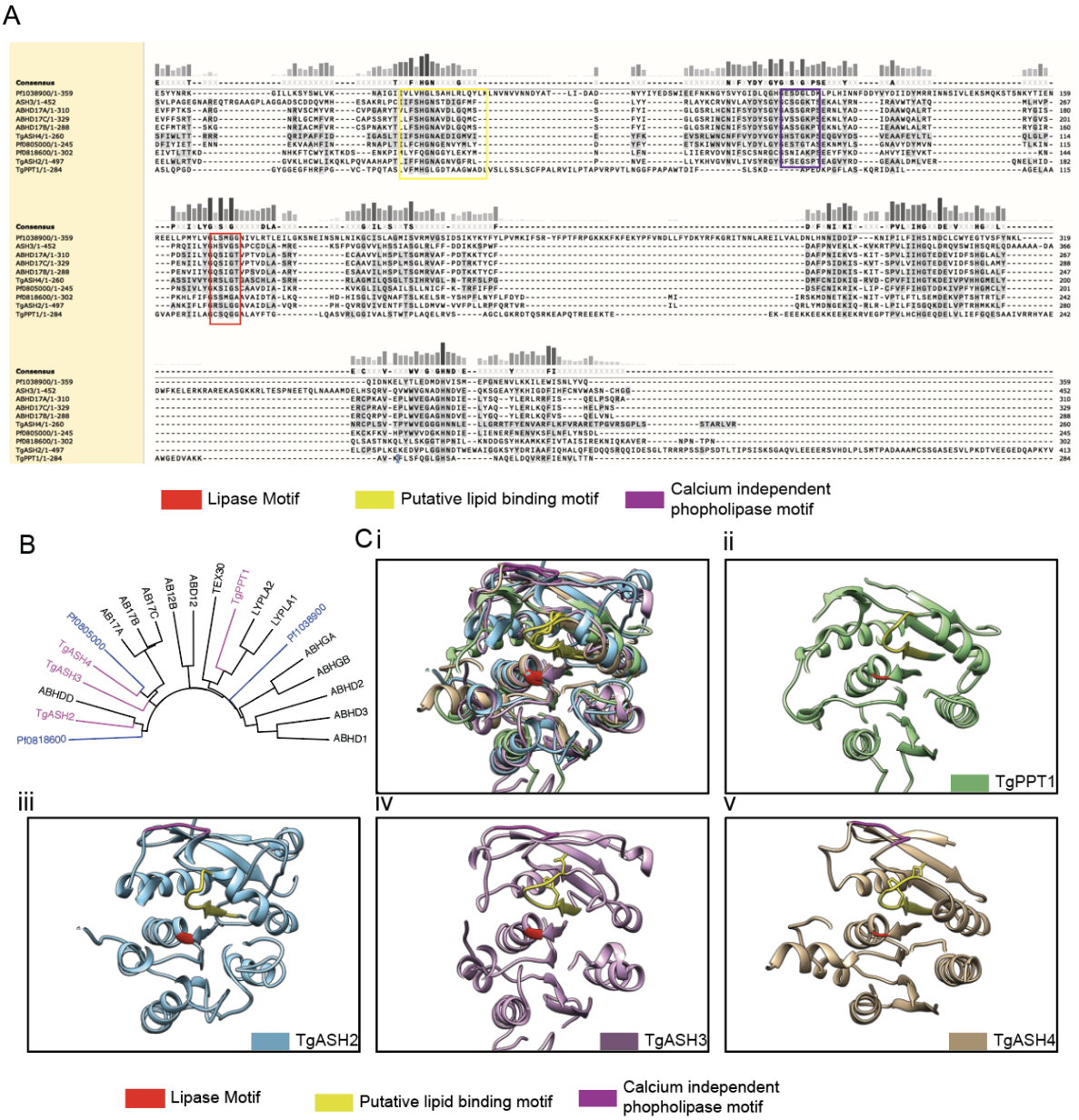

Supplementary Figure 1. Sequence analysis of T. gondii and P. falciparum serine hydrolases (related to Figure 1) (A) Sequence alignment of *Toxoplasma gondii* and *Plasmodium falciparum* serine hydrolases using Clustal Omega. Identical and highly similar residues are indicated within the conserved lipase motif (red), putative lipid binding domain (yellow) and calcium independent phospholipase motif (magenta). (B) Dendrogram of human, *T. gondii* and *P. falciparum* serine hydrolases showing the clustering in relation to human serine hydrolases (C). PyMOL structural modeling of *T. gondii* serine hydrolases using template structures (Table S1). The conserved lipase motif (red), putative lipid binding domain (yellow) and calcium independent phospholipase motif (purple) are highlighted. Images of (i) overlay of *Tg*PPT1 and *Tg*ASH2-4 (ii) *Tg*PPT1 (iii) *Tg*ASH2 (iv) *Tg*ASH3 and (v) *Tg*ASH4 homology models

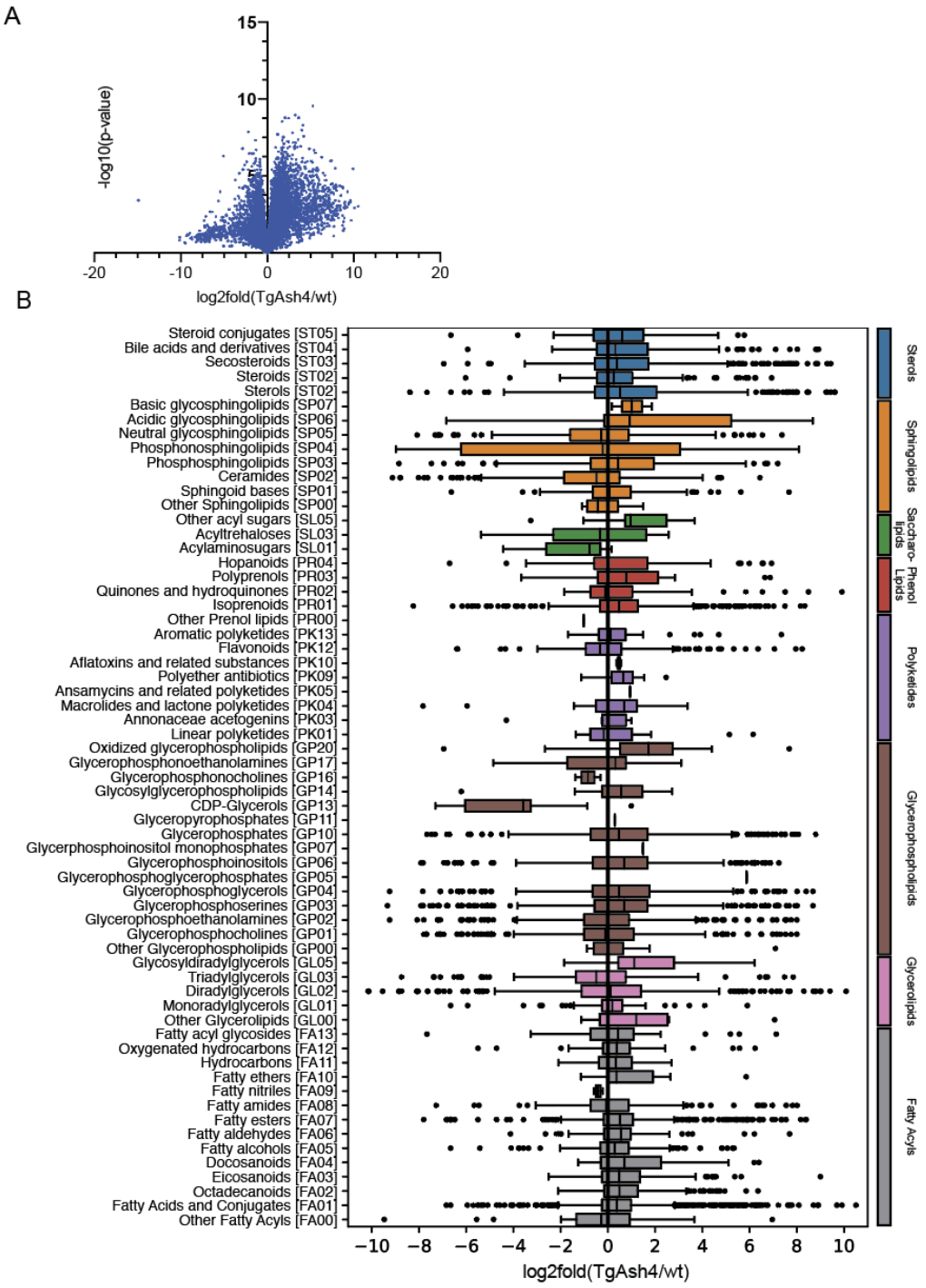

Supplementary Figure 2. Lipidomic analysis of ΔTgAsh4 and wild type parasite (related to Figure 4) Volcano plot showing log scaled mean fold change and adjusted p values for all the lipids resulting from the differential expression analysis between Δ*Tg*ASH4 and wild-type parasites (Figure 4C-E). (B) Box plot diagram highlighting the changes in the overall lipid species distribution in Δ*Tg*ASH4.

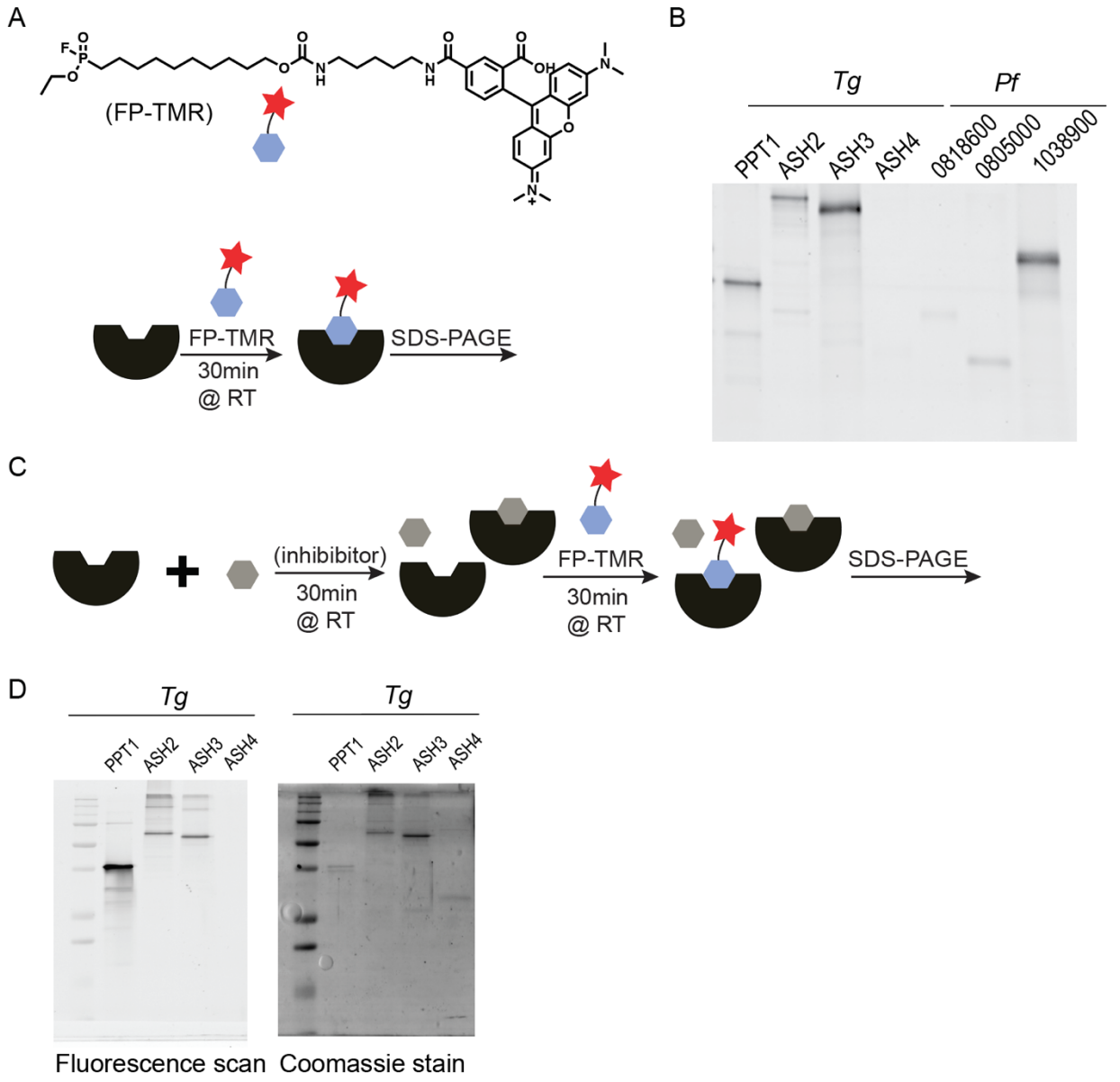

Supplementary Figure 3. Active site labeling of recombinant serine hydrolases with Fp-TMR. (Related to figure 5). (A) Structure of FP-TAMRA (upper panel) and schematic showing labeling of the enzymes with FP-TAMRA before analysis of SDS_PAGE gel (lower panel) (B) SDS-PAGE gel showing the FP-TAMRA labeling of the recombinant *T. gondii* and *P. falciparum* serine hydrolases. (C) Schematic showing the inhibitor screen set using competition labeling with FP-TMR. (D) Gel images of recombinantly expressed and purified TgPPT1, TgASH2, TgASH3 and TgASH4 labeled with FP-TAMRA and analyzed by SDS-PAGE followed by scanning of the gel for fluorescence (Left) or coomassie staining (right) to show purity of the proteins.

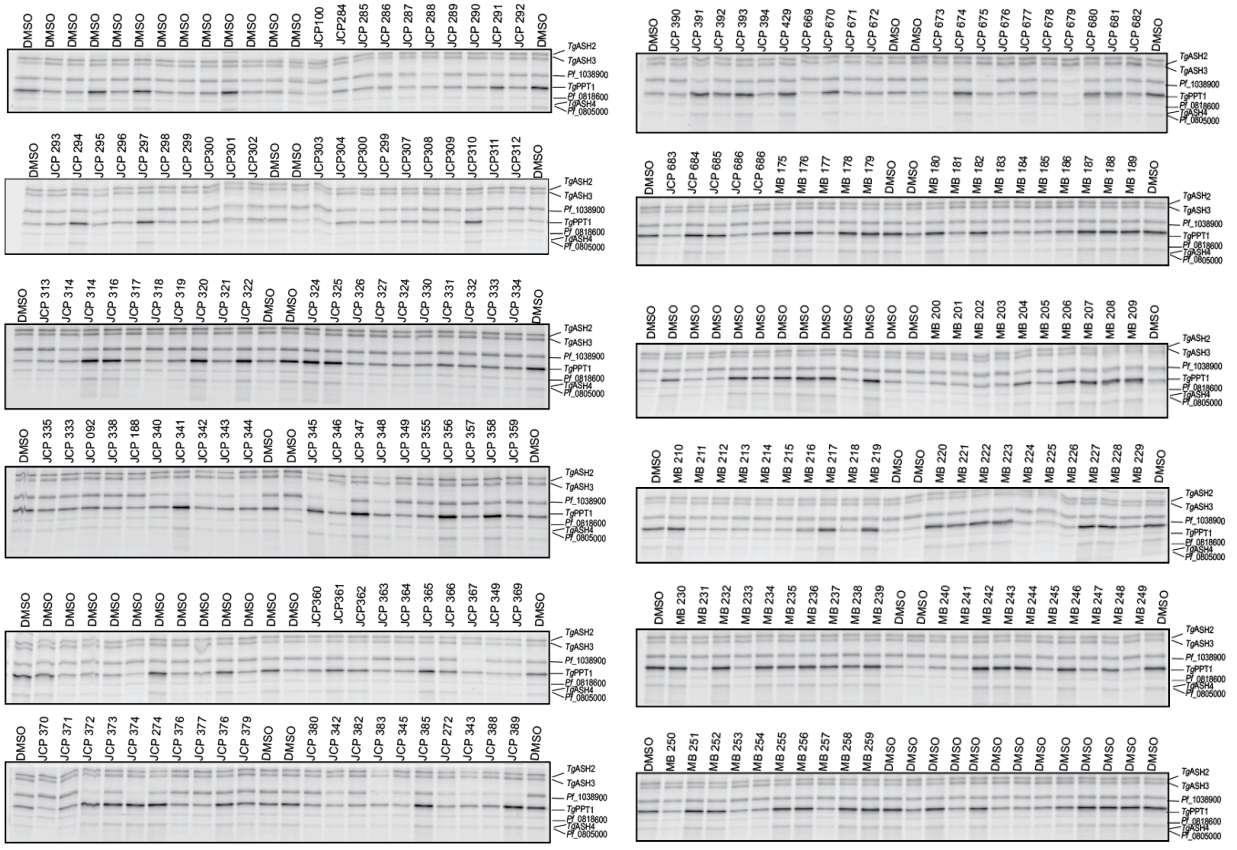

Supplementary Figure 4. (Related to Figure 5). SDS-PAGE gel based competitive activity-based protein profiling results showing inhibition of recombinant *T. gondii* and *P. falciparum* serine hydrolases. The enzymes were pooled and pre-incubated with 33μM of serine reactive compounds with and subsequent addition of FP-TAMRA. Competition was assessed using fluorescence intensity of SDS-PAGE gel bands.

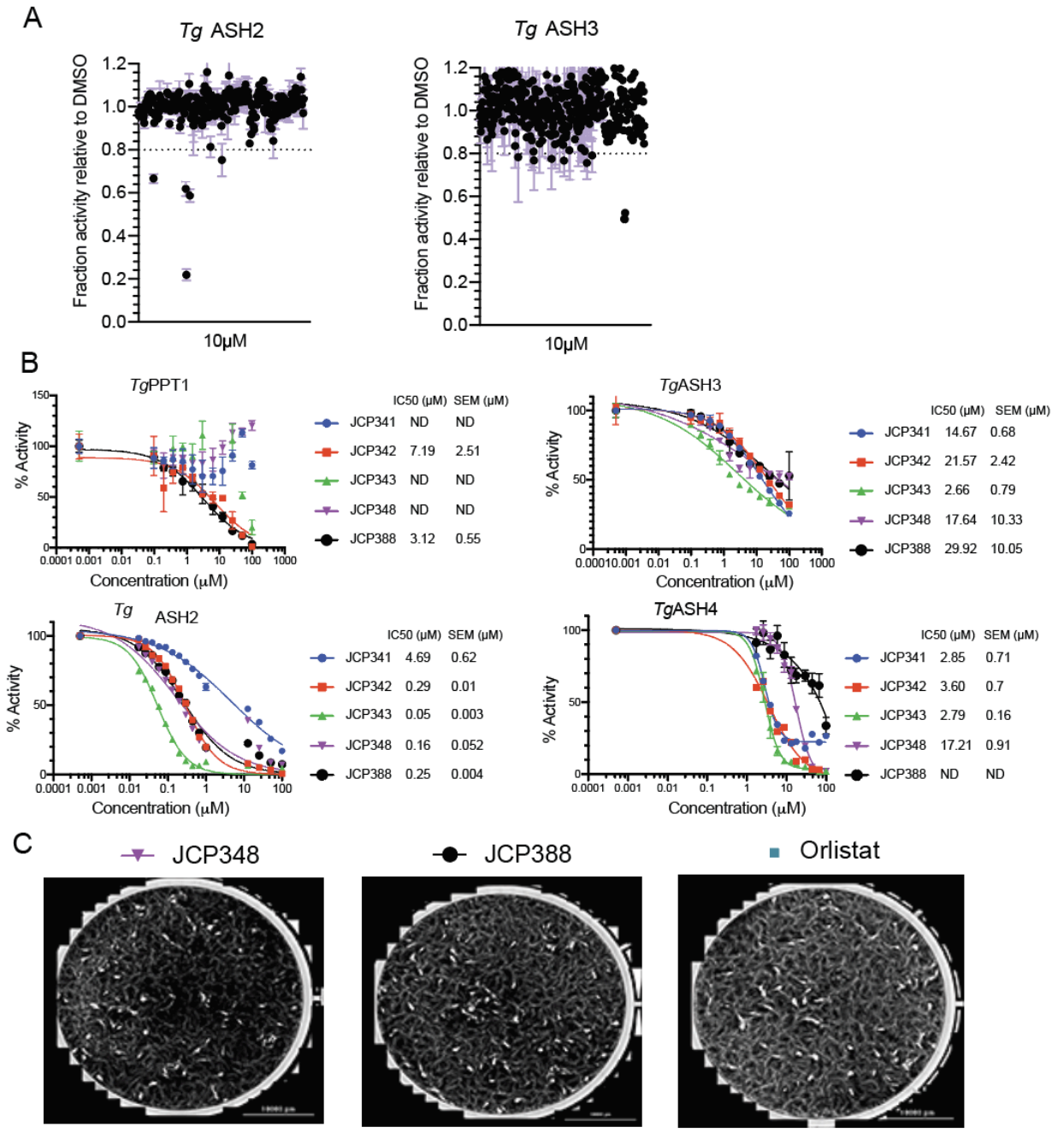

Supplementary Figure 5. (Related to Figure 6). (A) Dot plot showing our secondary screen inhibitors using a 4MU-octanote as the substrate (Figure 5B) and (B) Inhibitor validation in vitro and calculation of the IC50 curves and values of selected compounds (Figure 5B) (C) Inhibitor validation in cell culture infection model using a plaque assay that measures plaque formation by the wild type parasites in presence or absence of JCP341, JCP342, JCP343, JCP348, and Orlistat (Figure 6A, B).

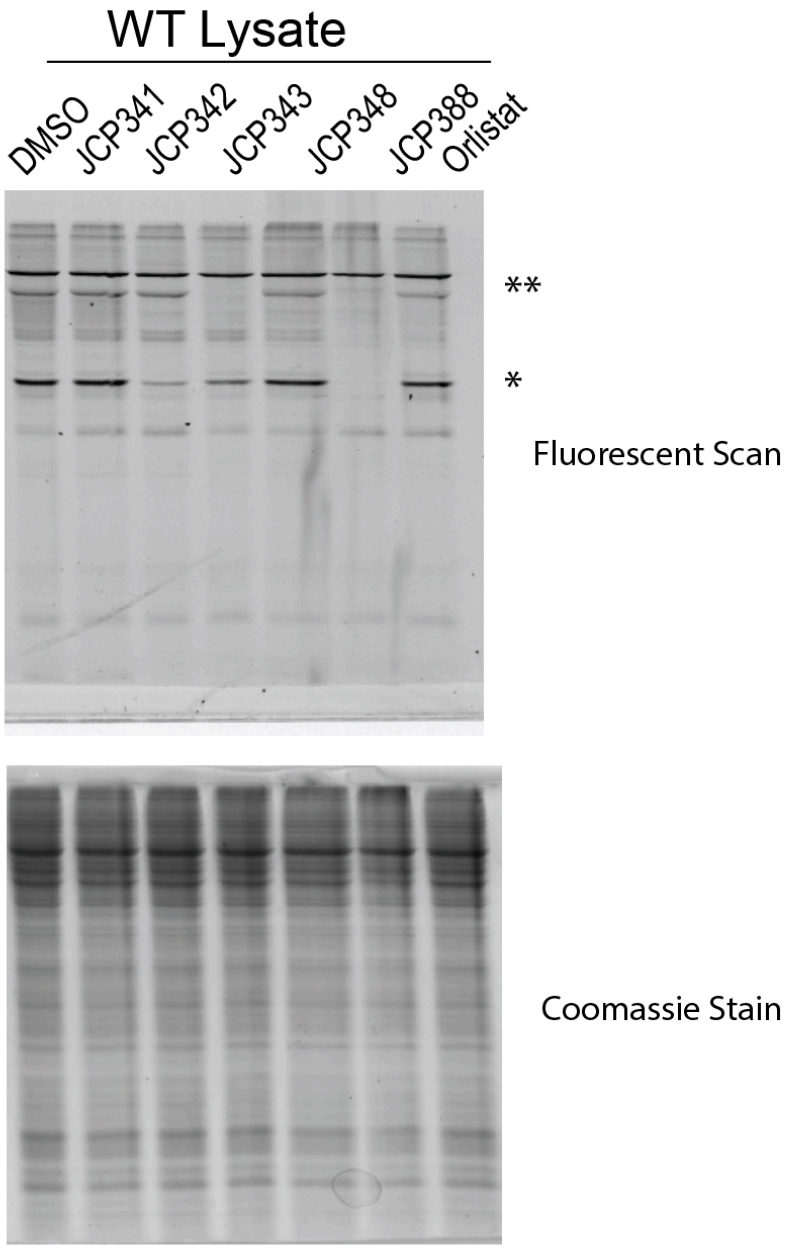

Supplementary Figure 6. **(Related to Figure 5).** ABPP competition of chloroisocoumarins hits targeting TgPPT1 and TgASH2-4 in total parasite lysates. Total detergent lysates from WT parasites were treated with each of the indicated screening hits at a final concentration of 10 μM at 37 degrees C. After 30 minutes, samples were labeled for 30 minutes with the FP-TAMRA probe (1μM final concentration) and samples resolved by SDS-PAGE. Images show fluorescent scan (top) and Coomassie stain (bottom) of the resulting gels.

Table S1. (Related to Figure 1). List of structural temples used to build homology models of serine hydrolases.

Enzyme	structural template	template type	sequence identity (%)	FFAS score	position of catalytic residues	remarks
*Tg*PPT1						
	5syn_A	thioesterase	36	-83.6	S128, D221, H263	analyzed model, position of docked substrate follow exper. position of inhibitor in the template structure**
	1fj2_A	thioesterase	34	-81.9		
	2wtm_A	EST1E	15	-26.8		not well defined binding pocket
*Tg*ASH2						
	6imp_A	RTX toxin, serine hydrolase	17	-65	S192, D268, H298	analyzed model**
	5g59_A	esterase	17	-52.9		second model**
	6ii2_A	putative RTX toxin	15	-31		catalytic triad not formed
*Tg*ASH3						
	6imp_A	RTX toxin, serine hydrolase	16	-61.8	S277, D346, H420	H420 not modelled, template too short
	5g59_A	esterase	15	-47.2		analyzed model**
	6ii2_A	putative RTX toxin	15	-29.9		catalytic triad not formed
*Tg*ASH4						
	6imp_A	RTX toxin, serine hydrolase	16	-66.4	S124, D188, H217	position of D188 incorrect
	5g59_A	esterase	20	-58.8		analyzed model**
	2wtm_A	EST1E	18	-37.6		not well defined binding pocket

Table S2. (Related to Figure 3). Kinetic parameters for the processing of lipid ester substrates by the recombinantly expressed hydrolase enzymes.

	TgPPT1	Km	Kcat	Kcat/Km
	Vmax	(μM)	(S^{-1})	S^{-1} M^{-1}
4MU(2)	60.039	79.99	0.15	1850.91
4MU(4)	51.48	12.89	0.13	9849.13
4MU(7)	19.61	153.98	0.05	314.06
4MU(8)	89.64	17.64	0.22	12531.66
4MU(10)	95.61	8.99	0.24	26237.29
	TgASH2	Km	Kcat	Kcat/Km
	Vmax	(μM)	(S^{-1})	S^{-1} M^{-1}
4MU(2)	129.32	62.30	0.32	5118.56
4MU(4)	62.91	12.94	0.16	11985.77
4MU(7)	31.66	3.76	0.08	20760.34
4MU(8)	14.14	3.55	0.03	9817.55
4MU(10)	6.36	18.13	0.016	864.95
	TgASH3	Km	Kcat	Kcat/Km
	Vmax	(μM)	(S^{-1})	
4MU(2)	158.86	77.81	0.39	5035.15
4MU(4)	53.17	21.12	0.13	6206.71
4MU(7)	10.13	61.26	0.025	407.82
4MU(8)	2.95	12.93	0.01	562.19
4MU(10)	ND	ND	ND	ND
	TgASH4	Km	Kcat	Kcat/Km
	Vmax	(μM)	(S^{-1})	S^{-1} M^{-1}
4MU(2)	138.83	108.81	0.34	3146.42
4MU(4)	42.07	33.33	0.10	3113.17
4MU(7)	6.27	59.19	0.02	261.31
4MU(8)	1.82	48.34	0.0045	92.89
4MU(10)	ND	ND	ND	ND